UPFLOWS IN FUNNEL-LIKE LEGS OF CORONAL MAGNETIC LOOPS

HUI TIAN[1,2], ECKART MARSCH[2], WERNER CURDT[2], AND JIANSEN HE[2]

[1] School of Earth and Space Sciences, Peking University, 100871, Beijing, China; tianhui924@gmail.com
[2] Max-Planck-Institut für Sonnensystemforschung, 37191, Katlenburg-Lindau, Germany

ABSTRACT

The prominent blueshifts of Ne VIII associated with the junctions of the magnetic network in the quiet Sun are still not well understood. By comparing the coronal magnetic-field structures as obtained by a potential-field reconstruction with the conspicuous blueshift patches on the Dopplergram of Ne VIII as observed in an equatorial quiet-Sun region, we find that most of the regions with significant upflow are associated with the funnel-like legs of magnetic loops and cospatial with increments of the line width. These quasi-steady upflows can be regarded as the signatures of mass supply to coronal loops. By using the square root of the line intensity as a proxy for the plasma density, the mass flux of the upflow in each funnel can be estimated. We find that the mass flux is anti-correlated with the funnel's expansion factor as determined from the extrapolated magnetic field. One of the loop systems is associated with a coronal bright point, which was observed by several instruments and exhibited various morphologies in different wavelengths and viewing directions. A remarkable agreement between its magnetic structure and the associated EUV emission pattern was found, suggesting an almost potential-field nature of the coronal magnetic field. We also report the direct detection of a small-scale siphon flow by both *STEREO* satellites. However, this transient siphon flow occurred in a weak mixed-polarity-field region, which was outside the adjacent magnetic funnel, and thus it is perhaps not related to plasma upflow in the funnel. Based on these observations, we suggest that at upper transition region (TR) temperatures the dominant flows in quiet-Sun coronal loops are long-lasting upflows rather than siphon flows. We also discuss the implications of our results for coronal heating and unresolved magnetic structures.

Key words: Sun: corona – Sun: magnetic fields – Sun: transition region – Sun: UV radiation

Online-only material: color figures, animations

1. INTRODUCTION

Quasi-steady flows have been frequently observed everywhere in the upper solar atmosphere, and the apparent steadiness of the global flow pattern seems to indicate a systematic large-scale plasma circulation in the solar corona and transition region (TR; Foukal 1978; Marsch et al. 2004, 2008; Dammasch et al. 2008). It is well known, but not yet fully understood, that in the network of the quiet Sun the ultraviolet emission lines formed in the TR are redshifted by a few km s^{-1} (e.g., Doschek et al. 1976; Brekke et al. 1997; Chae et al. 1998b; Curdt et al. 2008). As the temperature increases, the observed average Doppler shift turns from a red into a blueshift in the upper TR (Peter & Judge 1999; Xia et al. 2004). Recently, EUV Imaging Spectrometer (EIS; Culhane et al. 2007) observations showed that coronal lines revealed high outflow velocities on the order of 100 km s^{-1} in a compact region (network boundary) of the quiet Sun (Dere et al. 2007).

The Ne VIII (770.4 Å) line is formed in the upper TR and lower corona, and is on average blueshifted in coronal holes and the quiet Sun (e.g., Dammasch et al. 1999). In coronal-hole Dopplergrams, sizable patches of blueshift were frequently reported and usually interpreted as indicators of solar wind outflow (Hassler et al. 1999; Stucki et al. 2000; Wilhelm et al. 2000; Xia et al. 2003; Aiouaz et al. 2005; Tu et al. 2005a). In the quiet Sun, significant blueshifts of Ne VIII were also found at the network junctions and considered to be possible sources of the solar wind (Hassler et al. 1999). However, through a combined analysis of and comparison between three-dimensional (3D) magnetic-field structures and EUV observations, He et al. (2007) and Tian et al. (2008b) found that most of the sites with Ne VIII blueshift were not located in open-field regions. Con-

sequently, they argued that these sites might not be sources of the solar wind. Furthermore, Tian et al. (2008b) also noted that there were some loops revealing upflows in both legs, and some other loops with upflow in one and downflow in the other leg.

Although the smaller coronal structures are not well resolved, many attempts have already been made to understand these magnetic-field structures above the photosphere. Gabriel (1976) suggested the first magnetic-network model, in which the TR emission originates from magnetic funnels diverging with height and originating from the underlying supergranular boundaries. This picture was modified by Dowdy et al. (1986) who suggested that only a fraction of the network flux shaped as a funnel opens into the corona, while the majority of the network is occupied by a population of low-lying loops. Peter (2001) suggested that there may be two types of funnels, namely the ones connected to the solar wind and those forming the feet of large loops. Recently, based on the observed vector magnetic field, Tsuneta et al. (2008) proposed that the height where the funnel expands dramatically is higher in the quiet Sun than in coronal holes. On the other hand, magnetic-field extrapolation is a common method for the solar community to construct the coronal field and study the magnetic coupling of different solar processes (Wiegelmann & Neukirch 2002). The linear force-free model as proposed by Seehafer (1978) has been successfully applied before to study coronal holes and quiet-Sun regions (Wiegelmann et al. 2005; Tu et al. 2005a, 2005b; Marsch et al. 2006; He et al. 2007; Tian et al. 2007, 2008b).

In this paper, we present new observational results and further investigate the magnetic coupling and guidance of the plasma flows in the corona and TR. The results are discussed and interpreted in the context of coronal circulation.
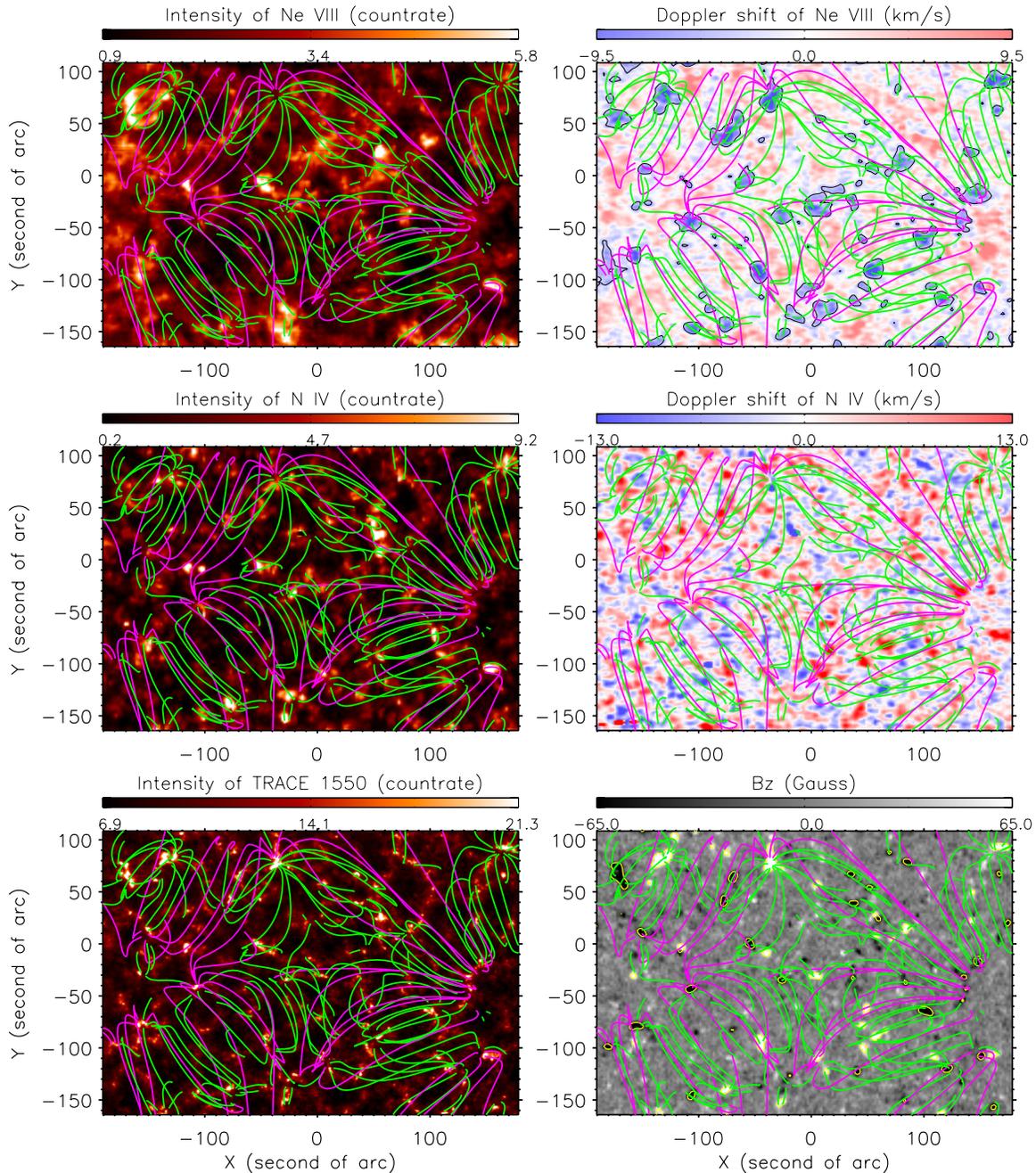
Figure 1. Projections onto the *x–y*-plane of the extrapolated magnetic-field lines, being superposed on the maps of the intensity and Doppler shift of Ne VIII (upper panels) and N IV (middle panels), the intensity of *TRACE* 1550 Å (lower left), and the photospheric longitudinal magnetic field strength (lower right). Field lines reaching higher and lower than 40 Mm are plotted in purple and green, respectively. Patches with significant blueshift (larger than 3 km s^{-1}) are outlined by the filled contours on the Dopplergram of Ne VIII. In the magnetogram, the strong-field (larger than 40 G in field magnitude) regions are outlined in yellow.

(A color version of this figure is available in the online journal.)

2. ULTRAVIOLET OBSERVATIONS AND MAGNETIC-FIELD EXTRAPOLATION

The Solar Ultraviolet Measurements of Emitted Radiation (SUMER; Wilhelm et al. 1995; Lemaire et al. 1997) data analyzed here were acquired at the disk center from 13:24 to 16:00 UT on 2008 July 3. The slit 2 ($1'' \times 300''$) was used to scan an area with a size of about $370'' \times 300''$ in this observation sequence. Spectra of Ne VIII ($\lambda 770.4$) and several other TR lines including N IV ($\lambda 765.1$) were recorded on detector B with an exposure time of 60 s. The standard SUMER procedures for correcting and calibrating the data were applied. They

include decompression, flat-field correction, and corrections for geometrical distortion, local gain, and dead time. By applying a single-Gaussian fit to each spectrum, the intensity map and Dopplergram of Ne VIII were obtained and presented in Figure 1.

During the SUMER observation, full-disk magnetograms with a one-minute cadence and $2''$ pixel size were obtained by Michelson Doppler Imager (MDI; Scherrer et al. 1995) onboard *Solar and Heliospheric Observatory* (*SOHO*). We found that the magnetogram was quite stable and showed almost no change during the period of the SUMER observation. In order to increase the signal-to-noise ratio, seven magnetograms observed from 15:00 to 15:06 UT were averaged. The coalignment

between SUMER and MDI images was achieved through a cross-correlation between the radiance map of N IV and the averaged magnetogram. The coaligned magnetogram can be found in Figure 1. A subregion with a size of 120″, being larger than the SUMER observation region, was extracted from the averaged magnetogram and then used to build a 3D potential magnetic field, which is based on the model proposed by Seehafer (1978). In Figure 1, the projections of the extrapolated magnetic loops onto the *x*–*y*-plane have been plotted on the different images. In order to obtain a better view of the complicated magnetic-field structure, the field lines reaching higher and lower than 40 Mm are plotted in purple and green, respectively.

In Figure 1, a *Transition Region and Coronal Explorer* (*TRACE*) image (Handy et al. 1999) was also shown to reveal the chromospheric network pattern. It is an average of 100 frames observed from 14:00 to 15:09 UT in the 1550 Å passband. The images have a pixel size of 0″.5. Before averaging, the standard software for reducing *TRACE* data was applied to the images, and the satellite jitter was subsequently removed by applying the cross-correlation technique. The coalignment between *TRACE* and MDI images was done through cross-correlation (note that the *SOHO* spacecraft was rotated at this time).

STEREO data were also available during this period. The separation angle between the two spacecraft was 59° and thus allowed for a stereoscopic study of some of the events and structures in the quiet Sun. The data obtained from 12:00 to 17:00 UT by the two almost identical SECCHI/EUVI telescopes (Wuelser et al. 2004) in all the four passbands were reduced by using the procedure *SECCHI_prep.pro* available in SSW (SolarSoft).

3. RESULTS AND DISCUSSION

3.1. Continuous Mass Supply to Magnetic Funnels

The prominent blueshifts of Ne VIII associated with network junctions in the quiet Sun were first reported by Hassler et al. (1999). However, so far the meaning of this blueshift and its relationship with the persistent redshift in lines at lower temperatures have not been understood. Tian et al. (2008b) revisited the middle-latitude quiet-Sun data analyzed before by Hassler et al. (1999). With the help of magnetic-field extrapolation, they found that most of the blueshifts seem to be associated with the legs of magnetic loops, and most likely indicate plasma outflow into and mass supply to coronal loops.

From our Figure 1, we find that almost all of the patches that have a significant blueshift on the Dopplergram of Ne VIII coincide with legs of loops located at network junctions. Thus, we confirm the previous finding in Tian et al. (2008b), who also noted that there are loops revealing large blueshifts in both legs, and some loops with upflow in one and downflow in the other leg. However, from Figure 1 we can see now that most of the blueshift patches coincide with both legs of magnetic loops, and some patches are associated with the common leg of several joint loops. Loop legs may generally be shaped in the form of funnels. Peter (2001) proposed a TR structure, in which magnetic funnels can either be connected to the solar wind, or form the legs of large coronal loops. In this picture, one funnel just corresponds to one leg of a single loop. However, in Figure 1 we find that a single funnel can in fact be a common leg of several joint loops with different spatial scales and orientations. Thus, the mass and energy flowing into a single funnel can then be spread and supplied to multiple loops. In some cases, the flows

in different loops may have different velocities and thus reveal several sub-patches of blueshift within one blueshift patch on the Dopplergram of Ne VIII.

Marsch et al. (2008) proposed the concept of coronal circulation, or convection to use a more apt term first coined by Foukal (1978), to emphasize that the plasma in the corona is nowhere static but everywhere flowing, being thereby guided by various magnetic channels. Many kinds of flow appear to be long lasting on large scales, and thus may indicate quasi-steady plasma convection encompassing and affecting the entire corona and TR. In particular, the blueshifts of Ne VIII at the network junctions are observed to be long lasting, and thus should play a permanent role in the process of coronal mass circulation. It is interesting to note that in the network of the quiet Sun the ultraviolet emission lines formed in the TR are usually redshifted by a few km s^{-1} (e.g., Doschek et al. 1976; Brekke et al. 1997; Chae et al. 1998b; Curdt et al. 2008). This phenomenon can be seen in the Dopplergram of N IV as presented in Figure 1. Here the Doppler shift was determined by assuming a net average shift of zero in the entire region. The origin of this redshift is still under debate (see reviews in Mariska 1992; Brekke et al. 1997). From Figure 1 it is clear that most loop legs are associated with patches of strong N IV redshift. However, the strongest redshifts of N IV do not fully coincide with but slightly deviate from the strongest blueshifts of Ne VIII, which was found previously by Aiouaz (2008) and Tian et al. (2008c).

Also, the relationship between the redshift of cool lines and blueshift found at higher temperatures is not well understood. In coronal holes, the contemporaneous and adjacent red and blueshifts were explained as indicating downflow and upflow after magnetic reconnection between open-field lines in coronal funnels and their side loops (Axford et al. 1999; Tu et al. 2005a; He et al. 2008). In the quiet Sun, the scenario of continuous reconnection might also apply, if the magnetic polarities of side loops are opposite to those of funnel-like loop legs (McIntosh et al. 2007; Tian et al. 2008b; Aiouaz 2008), thus enabling reconnection.

There might be another possibility: a cool plasma (in the photosphere and chromosphere) might continuously enter any loop leg through a certain process (e.g., diffusion) from outside, but then flow up and speed up after heating occurred. At the height of the upper TR, this flow becomes significant and may lead to a strong blueshift of the emission lines formed there. Due to the onset of possible (radiative) cooling effects (e.g., Kamio et al. 2009), the flow might again decelerate above a certain height (perhaps in the lower corona) and finally turn downward and accelerate under gravity, which may lead to emission by the dense plasma at lower temperatures and then cause the redshift of TR lines. The steadiness of the observed shifts suggests that all these processes should occur continuously and persistently. However, since the density decreases with height, the contribution of the cooling plasma to the observed redshift at TR temperatures might be minor, as compared to that of the downward plasma resulting from reconnection.

3.2. Relationship Between Mass Flux and Expansion Factor

As mentioned in Tian et al. (2008b), we can estimate the rate of mass supply to a coronal loop if we accept the Doppler shift of Ne VIII as a proxy for the plasma bulk flow (i.e., of the proton flow). The mass flux can be calculated as $f = N_e V A$, where N_e, V, and A represent electron density, outflow velocity, and the area of an observed blueshift patch. Here we have selected 21 patches with significant blueshifts, which are clearly associated with

Table 1
Parameters Derived from the Dopplergram and Intensity Image of Ne VIII, and from the Extrapolated Magnetograms

Position (x'', y'')	V (km s^{-1})	A (Mm^2)	I (count rate)	B_z at 0 Mm (G)	B_z at 4 Mm (G)
−175, 55	5.11	165.57	3.80	83.70	32.3
−130, 75	5.80	237.46	3.06	123.7	50.1
−80, 35	6.01	141.60	2.73	74.90	22.0
−35, 75	7.13	196.07	2.40	118.9	45.8
−145, 5	4.95	54.464	3.31	66.60	18.5
−110, −50	5.39	156.85	2.26	91.20	24.3
−160, −75	5.62	76.250	3.40	73.60	20.8
−75, −145	4.79	78.428	3.35	68.60	18.7
−45, −95	7.50	128.53	2.14	67.20	23.5
−25, −40	5.05	115.46	2.58	64.70	16.4
−60, −10	4.67	119.82	2.62	83.70	20.4
55, −90	7.04	143.78	2.61	69.60	23.5
100, −60	5.68	152.50	2.18	92.60	27.1
115, −120	4.51	108.92	3.00	97.00	24.7
150, −110	4.84	56.643	3.08	83.30	19.4
145, −20	4.55	215.67	2.22	81.30	24.5
165, 90	6.92	150.32	2.97	89.30	26.4
80, 10	4.55	189.53	2.86	69.20	20.0
135, −40	4.24	95.857	2.87	72.70	21.5
−5, −110	4.03	91.500	2.30	58.50	17.0
10, −130	4.38	174.28	1.91	52.20	14.6

Notes. V and I are the average velocity and intensity in each blueshift patch with area A. B_z represents the magnitude of the longitudinal component of the extrapolated magnetic field vector.

funnel-like loop legs, as inferred from Figure 1. For each case, we selected the region where the blueshift is larger than 3 km s^{-1}, by plotting contours on the Dopplergram, and then calculated A and the average V. For our studied region, we could not make a direct density measurement by using the available data. However, under the assumption of the same thermal structure, we can evaluate the electron density by using the square root of Ne VIII line intensity (Xia 2003; Marsch et al. 2004). Since the Mg VII and Ne VIII lines have a similar formation temperature, we adopted a value of $N_e = 10^{8.95}$ cm^{-3}, from the density measurement by using Mg VII in Landi & Landini (1998).

By assuming this value for the average density of our studied region, we got a scaling factor between the electron density and the square root of the intensity. We then superposed contours of the Doppler shift on the intensity image and thus obtained the average intensity I within each contour. By use of the scaling relation, we got the values of the electron density. The values of V, A, I, and the approximate coordinates of all cases analyzed are listed in Table 1. We have to mention that the Doppler shift was determined by assuming a net average shift of zero in the entire region. Since the average Doppler shift of Ne VIII is about 2 km s^{-1} (blueshift) in the quiet Sun (Peter & Judge 1999; Xia et al. 2004), we simply added 2 km s^{-1} to V before we calculated the mass flux for each case.

The information on the 3D coronal magnetic field, as obtained by an extrapolation of the measured photospheric magnetic field, allows one to study the geometry of magnetic flux tubes in the corona. Since plasma flows are guided by magnetic flux tubes, the expansion of a tube might play an important role in the process of coronal mass supply. Since the magnetic flux is conserved along a flux tube, we can calculate the expansion factor of the tube (see, e.g., Marsch et al. 2004) if the values of magnetic field strength at different heights in the tube are known. Here we aimed at a calculation of the expansion factor of each funnel-like loop leg below 4 Mm. The selection of

4 Mm is based on the estimation of Ne VIII emission height in the quiet Sun (Tu et al. 2005b).

On the magnetogram shown in Figure 1, strong-field regions (larger than 40 G in magnitude) in the photosphere are outlined in yellow. For each selected patch of blueshift on the Dopplergram, it is easy to find the associated flux tube (strong-field region) on the magnetogram. These contours were then superposed on the extrapolated magnetogram at 4 Mm. We calculated the average values of the longitudinal magnetic field strength (B_z) in all contours which are associated with the selected funnels. Table 1 lists the results. The ratio of B_z at 0 Mm and 4 Mm is a measure of the area ratio between these two heights, the requested expansion factor.

Figure 2 presents a scatter plot of the mass flux versus the expansion factor for different magnetic funnels. The dashed line is a linear fit to the scattered data points. We can conclude that there is a declining trend of the mass flux with the increasing expansion factor. It is known that the source regions of fast solar wind, the polar coronal holes, are characterized by a relatively slow flux tube expansion. Typical sources of the slow solar wind are the many small holes located adjacent to active regions and the boundaries of polar holes, where rapidly diverging fields are known to be dominant (see a review in Wang 2009). The relationship between mass flux and the expansion factor here is similar to the well-known relationship between the wind speed and expansion factor. Thus a similar explanation might apply to both cases, although the spatial scales are different. In a rapidly diverging magnetic funnel, most of the energy that is brought in by the cool plasma and produced in heating processes may be deposited in a lower layer of the funnel (below the formation height of Ne VIII), and therefore the energy used to drive the upflow will be reduced. In contrast, if the expansion of the funnel is not significant, more energy will become available to accelerate the upflow, and thus the upward mass flux will be increased.
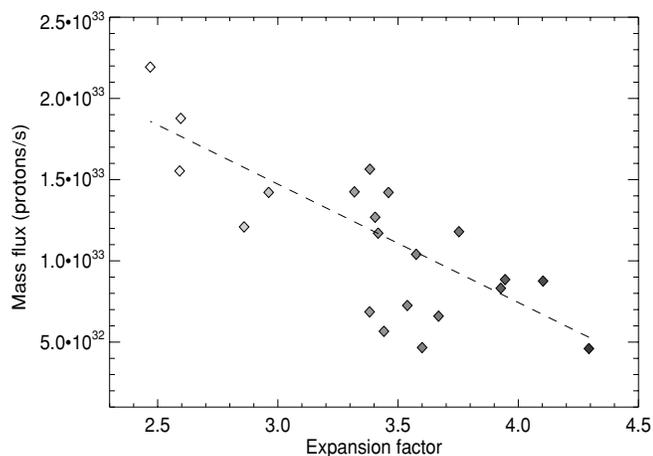
Figure 2. Scatter plot of the mass flux vs. expansion factor for different magnetic funnels. The dashed line is a linear fit to the scattered data points.

3.3. Upflows in Coronal Bright Point

Coronal bright points (BPs) are characterized by locally enhanced emission in X-ray, EUV, and radio wavelengths, and related to bipolar magnetic fields at network boundaries (Habbal et al. 1990; Webb et al. 1993; Falconer et al. 1998; Brown et al. 2001; Madjarska et al. 2003). It is believed that BPs are associated with small-scale (typically 30″–40″ in size) loop structures (Sheeley & Golub 1979; Tian et al. 2007; Péter-Suárez et al. 2008).

In our field of view, we found a typical BP, located and visible in the upper left corner of all panels of Figure 1, where we can see a magnetic loop system with both legs being anchored in the magnetic network. The BP shows enhanced emission in the intensity map of Ne VIII. The most interesting feature here is that upflows are seen in both legs of the loop system (upper right panel). Recently, Brosius et al. (2007) reported upflow and downflow on opposite sides of a BP, which was explained as the result of magnetic reconnection. Tian et al. (2008a) found a BP which revealed a totally different upflow/downflow boundary at lower and higher temperatures, suggesting a twist of the associated magnetic loop system. According to our knowledge, this is the first time that upflows are found in both legs of a BP loop system. This Doppler-shift pattern is not strange, since the BP is associated with a magnetic loop, which should not be too different from other loop structures, although this BP loop is of smaller size. Thus we may conclude that the blueshift of Ne VIII seen in both legs of the BP loop system is more likely a signature of mass supply to these loop, rather than a signature of solar wind origin. Our conclusion is consistent with the one made earlier by Wilhelm et al. (2000) and Xia et al. (2003), who concluded that BPs do not directly contribute to solar wind outflow. However, other authors suggested that BPs could be associated with jets (e.g., Shibata et al. 1996; Yokoyama & Shibata 1996) and might contribute to the high-speed solar wind in coronal holes (Cirtain et al. 2007). In the quiet Sun, if magnetic-field lines are transiently open, then their interactions with emerging flux can produce BPs and jets, releasing a plasma into the outer corona and solar wind. More studies are needed to investigate the role of BPs in solar wind origin.

The EUVI/SECCHI images presented in Figure 3 reveal the varying morphology of the BP when seen from two different viewing angles. The general emission patterns of the BP in the three passbands did not change during the period of SUMER observation, although the fine structures were rather dynamic. A comparison between the extrapolated magnetic structure and the BP emissions as seen by EUVI, *TRACE*, and SUMER suggests a remarkable agreement and thus indicates an almost steady, potential-like nature of the magnetic field. Our finding confirms the result of Péter-Suárez et al. (2008), who found an agreement between the extrapolated magnetic field configuration and some of the loops composing the BP as seen in the X-ray images and suggested that a large fraction of the magnetic field in the BP is close to being a potential field. The remarkable agreement here also suggests the suitability of the potential-field model for our study.
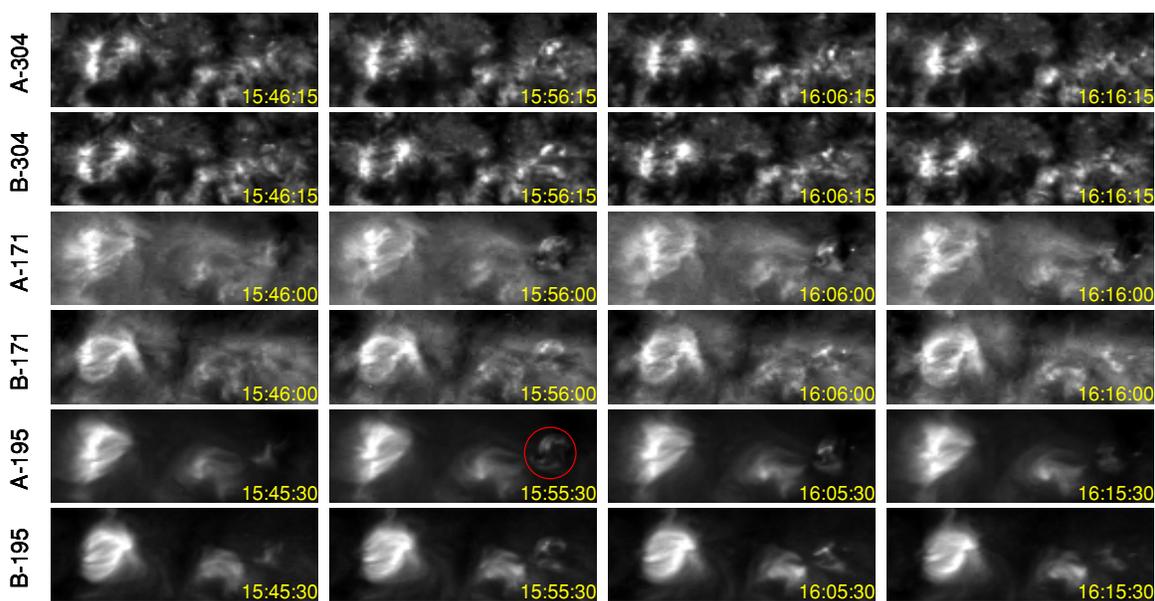
Figure 3. Time sequences of EUVI images taken in three passbands on the two *STEREO* spacecraft. The observation time is shown in the lower right corner of each image. The field of view corresponds approximately to an *x*-coordinate range from −200″ to 40″ and a *y*-coordinate range from 20″ to 120″. The red circle indicates the position of the transient siphon flow. Movies showing the evolution of the emissions in all four passbands of EUVI can be found in the online version of the journal.

(A color version and animations [A, B, C, D] of this figure are available in the online journal.)
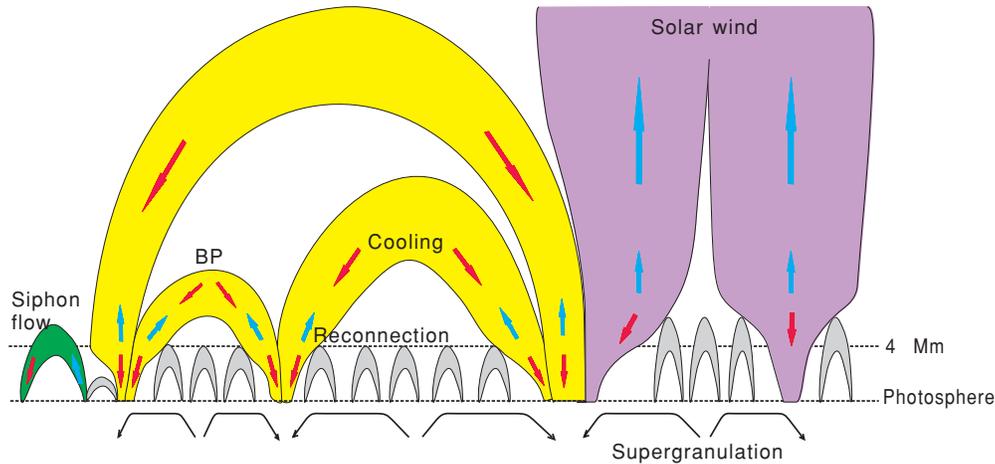
Figure 4. Schematic presentation of the flows in the magnetic structures of the quiet Sun. Magnetic loops with different scales and open-field regions are marked in different colors. Downflows and upflows are indicated by the red and blue arrows, respectively.

(A color version of this figure is available in the online journal.)

It is also clear that the emission pattern of the BP is different at different temperatures. At chromospheric temperatures, bright emission can be found only at the very bottom of loop legs, as seen in the *TRACE* 1550 Å image. With increasing temperature, from EUVI 304 Å, SUMER N IV, SUMER Ne VIII, EUVI 171 Å to EUVI 195 Å, more and more parts of the upper sections of the loop system are revealed. So it is difficult to identify the full loop structure from only one image. By inspection of Figure 3, we can also find that this BP is differently resolved into the various EUVI images onboard the two *STEREO* spacecraft, suggesting the importance of stereoscopic observations. As pointed out by Peter (2007), 3D models are important to account properly for the plasma and the magnetic-field structure as well as their interaction. Our results indicate, from an observational point of view, the importance of carrying out combined studies that use 3D observations at different temperatures and magnetic-field extrapolation for loop-like structures. The 3D reconstruction of active-region loops has been successfully done in the recent past (Feng et al. 2007). In principle, it should also be possible to reconstruct the 3D structure of a small-scale loop system that, e.g., is associated with a BP.

3.4. A Transient Siphon Flow Outside Magnetic Funnels

It is well known that the corona is rather dynamic, not only in active regions but also in the quiet Sun. Small-scale transient events have been reported frequently for the quiet Sun. In our data set we also found one case of a dynamic event, a transient siphon flow.

This siphon flow occurred approximately from 15:50 to 16:10 UT on the right side of a blueshift patch (the one with a coordinate of $(-35, 75)$ in Table 1). It was recorded in all of the four passbands of EUVI on both spacecraft. Movies showing the evolution of the emissions in the four passbands can be found online (note the different cadences in different passbands). We did not de-rotate the images since an interpolation might have smoothed out the small-scale event. Figure 3 only shows several snapshots. From the movie we can see bright emission features moving along two small parallel loops from one end to the other. The two loops were located in a weak mixed-polarity region on the magnetogram shown in Figure 1. They were rather small and cold before the occurring of the event, and thus were not properly resolved by EUVI. Due to the elevated temperature and

enhanced coronal emission resulting from an unknown heating process, the two cold loops were clearly seen during the period of the siphon flow, especially at around 15:55:30 in the 195 Å passband of EUVI onboard *STEREO-A*. Under the assumption of a semi-circular shape, the loop length can be estimated as $40''$. Then the speed of the flow can be calculated as 24 km s^{-1}.

Siphon flows are believed to be driven by asymmetric heating or pressure gradients between two legs of the loop (e.g., Robb & Cally 1992; Orlando et al. 1995). They have been frequently found in large active-region loops, but rarely been observed in the quiet Sun. Teriaca et al. (2004) identified a supersonic siphon-like flow in a quiet-Sun loop, by analyzing spectral profiles of O VI. Siphon flows in small loops in active regions were also detected by Uitenbroek et al. (2006) and Doyle et al. (2006). Here, we reported a direct observation of a small-scale siphon flow in the quiet Sun by both *STEREO* satellites. However, since this transient siphon flow occurred in a weak mixed-polarity field region and was outside the adjacent magnetic funnel, it should not be related to the long-lasting upflow in the funnel.

3.5. Flows in the Magnetic Structures of the Quiet Sun

Based on the above observations, we suggest a quiet-Sun magnetic structure which is presented in Figure 4. The cool loops, coronal loops, and open-field structures are marked in gray, yellow, and purple, respectively. Downflows and upflows guided by these structures are indicated by the red and blue arrows, respectively.

Cool loops with different spatial scales can be found in both network and internetwork regions. Legs of one or several large-scale magnetic structures (coronal loops or open-field structures) may be anchored in and crowd a network junction, forming a magnetic funnel. The internetwork loops are continuously swept through the supergranular convection to the network boundaries, where they may interact with the pre-existing funnels. These funnels can either be connected to the solar wind or form the legs of large coronal loops.

As mentioned previously, two mechanisms might be responsible for the systematic flows in coronal loops. Continuous reconnection between field lines in magnetic funnels and side loops is expected to produce upflows in the upper TR and downflows in the lower TR. The outflows produced by reconnections around

a funnel tend to converge toward the center of the funnel. In contrast, the hot plasmas trapped in low-lying loops are pulled down when they cool, and the downflows are stronger at the boundary of the network where side loops are accumulated. Thus, the bidirectional flows are likely to be detected as the not fully cospatial blueshift of Ne VIII and redshift of N IV. On the other hand, heating and cooling processes might also take place in quiet-Sun coronal loops. In most cases, upflows which are possibly caused by heating cannot reach the apices of the loops. When cooling is switched on, the flows turn downward and lead to emission at lower temperatures. This scenario will naturally explain the observational fact that most of the strongest redshifts of N IV do not fully coincide with the strongest blueshifts of Ne VIII, since the turning points are located in the curved segments of loop legs.

In classical pictures (e.g., Peter 2001), the dominant type of flow in coronal loops is siphon flow. However, our observation seems to indicate that siphon flow rarely exists in quiet-Sun coronal loops with a size comparable to or larger than a supergranule. In these large-scale loops, the upflowing plasma will get cooled and turn downward before reaching the apices. However, transient heating in one leg of a small loop may launch an upflow that can reach the apex and subsequently flow downward along the other leg of the loop. For BPs which are associated with magnetic loops of intermediate scales, these two types of flows may both exist.

The mass supplied into the coronal loops might also be released into the ambient corona or even into the solar wind. As claimed by He et al. (2007) and Tian et al. (2008b), sometimes quiet-Sun coronal loops might transiently open due to magnetic reconnection so that open-field lines forming magnetic funnels might also be present in the quiet Sun. These funnels originating from different network regions expand with height and finally merge into a single wide open-field region. The nascent solar wind is likely to be produced in these funnels, but at locations higher than the source of the Ne VIII emission. Recent EIS observations showed that coronal lines revealed high outflow velocities on the order of 100 km s^{-1} in a compact region (network boundary) of the quiet Sun (Dere et al. 2007). Future combined studies between magnetic-field extrapolation and spectroscopic observations including SUMER and EIS are needed to investigate whether this high-speed coronal outflow corresponds to the quiet-Sun solar wind or not.

3.6. Implications for Coronal Heating and Unresolved Magnetic Structures

EIS observations reveal hot plasma upflows of several tens km s^{-1} and enhanced nonthermal velocities near the footpoints of active-region loops (Hara et al. 2008). The authors claimed that this result supports the nanoflare heating model of Patsourakos & Klimchuk (2006) that treats a coronal loop as a collection of unresolved small-scale bundles. While based on a more recent finding that SUMER and EIS observations seem to show faint upflows at 50–100 km s^{-1} for temperatures from 100,000 to several million degrees, De Pontieu et al. (2009) suggested that the dominant part of coronal heating is provided by the chromospheric jets or type II spicules.

A heating process is usually associated with high-speed laminar flows, waves, or turbulent flows which all contribute to the nonthermal motion and tend to broaden the width of spectral lines (e.g., Hollweg 1984; Chae et al. 1998a; Tu et al. 1998). Thus, an investigation of the line width may provide
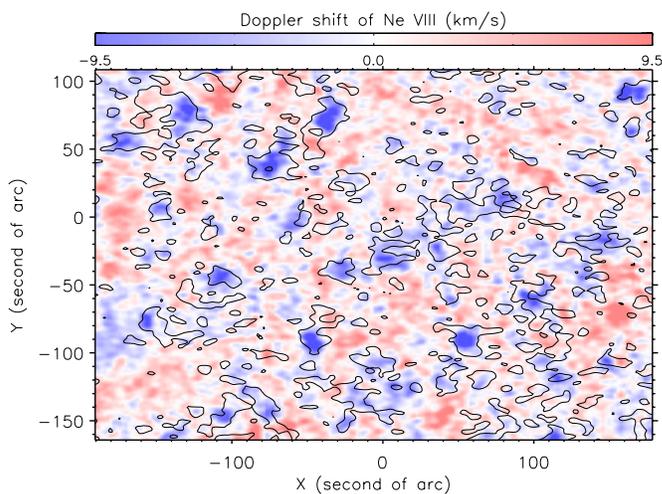
Figure 5. Contours of line width (top 20%) superposed on the Dopplergram of Ne VIII.
(A color version of this figure is available in the online journal.)

some implications for coronal heating. The correlation between the line radiance and nonthermal width for a certain TR line was investigated by Chae et al. (1998a). Here we found a similar result: the correlation coefficient is much higher for the typical TR line N IV (0.33) than for the upper TR line Ne VIII (0.13). Our most interesting result is that there is a high correlation between the line width and the Doppler shift of Ne VIII (correlation coefficient: −0.37; note that the blue and redshifts have negative and positive values, respectively). Contours of line width (top 20%) are superposed on the Dopplergram of Ne VIII in Figure 5. It is very clear that most of the significant blueshifts are associated with an enhancement of the line width.

Chae et al. (1998a) claimed that the superposition of different laminar flows in various unresolved loops cannot explain some observational characteristics of nonthermal motions. However, some model calculations led to a different conclusion. Multi-thread loop models suggested that a plasma from a single thread (strand) can have a very high speed, but since the initial rise of each thread is masked by threads that were heated previously and are emitting strongly, the composite emission from many strands in various stages of heating and cooling is dominated by the stationary emission (Warren & Doschek 2005; Patsourakos & Klimchuk 2006). According to this scenario, the plasma with a long-lasting blueshift of the order of 6 km s^{-1} in our observations should correspond to the stationary thermal emission in the upper TR of network junctions, while emission from some individual unresolved threads with high-speed motions corresponds to heating beams which yield increments of the line width but no detectable upflows at upper-TR temperatures. These high-speed upward plasmas may be associated with the chromospheric jets or type II spicules, which were suggested to be crucial for coronal heating in the mechanism proposed by De Pontieu et al. (2009). In our observation, most Ne VIII profiles are well approximated by a single Gaussian function and do not show visible asymmetries, which is consistent with previous observations and the nanoflare heating model of Patsourakos & Klimchuk (2006).

However, we have to keep in mind that the enhancement of the line width in network junctions may also be related to waves or turbulence, which are associated with the process producing the significant Ne VIII blueshift.

4. SUMMARY

Through a potential-field extrapolation, we have further investigated the coupling between solar magnetic structures and the prominent blueshifts of Ne VIII at the network junctions in the quiet Sun. An exceptionally clear and close relationship between the significant upflows and the funnel-like loop legs has been established. Moreover, we have made a first attempt to study the influence of the expansion factor of magnetic loops on the mass flux as inferred from spectroscopic observation and found an anti-correlation.

For the small-scale loop structure identified as coronal bright point, we have made the first combined study between the extrapolated magnetic field and 3D multi-temperature EUV observations. We find upflows in both legs of the loop system associated with the BP.

We also reported a direct detection of a transient siphon flow in the quiet Sun by both *STEREO* satellites. This siphon flow along two parallel small-scale loops occurred in a mixed-polarity-field region, which was located outside the adjacent magnetic funnel.

Based on these observations, we present in Figure 4 a new scenario of the flows guided by the quiet-Sun magnetic structures. In this scenario, the dominant flows at upper-TR temperatures in quiet-Sun coronal loops are long-lasting upflows rather than siphon flows. The mass supplied into and flows upward along coronal loops may fall downward again when cooling is switched on. Sometimes the coronal loops might transiently open due to magnetic reconnection and thus can release mass into the ambient corona or even into the solar wind.

Finally, we have recalled some recent results on the upflows in the TR and corona, and discussed the implications of our results for coronal heating. The significant correlation between the line width and Doppler shift of Ne VIII seems to favor a scenario of a magnetic funnel consisting of unresolved strands.

REFERENCES

Aiouaz, T. 2008, ApJ, 674, 1144
Aiouaz, T., Peter, H., & Lemaire, P. 2005, A&A, 435, 713
Axford, W. I., Mckenzie, J. F., & Sukhorukova, G. V. 1999, Space Sci. Rev., 87, 25
Brekke, P., Hassler, D. M., & Wilhelm, K. 1997, Sol. Phys., 175, 349
Brosius, J. W., Rabin, D. M., & Thomas, R. J. 2007, ApJ, 656, L41
Brown, D. S., et al. 2001, Sol. Phys., 201, 305
Chae, J., Schühle, U., & Lemaire, P. 1998a, ApJ, 505, 957
Chae, J., Yun, H. S., & Poland, A. I. 1998b, ApJS, 114, 151
Cirtain, J. W., et al. 2007, Science, 318, 1580
Culhane, J. L., et al. 2007, Sol. Phys., 243, 19
Curdt, W., Tian, H., Dwivedi, B. N., & Marsch, E. 2008, A&A, 491, L13
Dammasch, I. E., Curdt, W., Dwivedi, B. N., & Parenti, S. 2008, Ann. Geophys., 26, 2955
Dammasch, I. E., Wilhelm, K., Curdt, W., & Hassler, D. M. 1999, A&A, 346, 285
De Pontieu, B., McIntosh, S. W., Hansteen, V. H., & Schrijver, C. J. 2009, ApJ, 701, L1
Dere, K. P., et al. 2007, PASJ, 59, S721
Doschek, G. A., Bohlin, J. D., & Feldman, U. 1976, ApJ, 205, L177
Dowdy, J. F., Jr., Rabin, D., & Moore, R. L. 1986, Sol. Phys., 105, 35
Doyle, J. G., et al. 2006, A&A, 452, 1075
Falconer, D. A., Moore, R. L., Porter, J. G., & Hathaway, D. H. 1998, ApJ, 501, 386
Feng, L., et al. 2007, ApJ, 671, L205
Foukal, P. 1978, ApJ, 223, 1046
Gabriel, A. H. 1976, Phil. Trans. R. Soc. A, 281, 575
Habbal, S. R., Dowdy, J. F., Jr., & Withbroe, G. L. 1990, ApJ, 352, 333
Handy, B. N., et al. 1999, Sol. Phys., 187, 229
Hara, H., et al. 2008, ApJ, 678, L67
Hassler, D. M., et al. 1999, Science, 283, 810
He, J.-S., Tu, C.-Y., & Marsch, E. 2007, A&A, 468, 307
He, J.-S., Tu, C.-Y., & Marsch, E. 2008, Sol. Phys., 250, 147
Hollweg, J. V. 1984, ApJ, 277, 392
Kamio, S., Hara, H., Watanabe, T., & Curdt, W. 2009, A&A, 502, 345
Landi, E., & Landini, M. 1998, A&A, 340, 265
Lemaire, P., et al. 1997, Sol. Phys., 170, 105
Madjarska, M. S., Doyle, J. G., Teriaca, L., & Banerjee, D. 2003, A&A, 398, 775
Mariska, J. T. 1992, The Solar Transition Region (Cambridge: Cambridge Univ. Press)
Marsch, E., Tian, H., Sun, J., Curdt, W., & Wiegelmann, T. 2008, ApJ, 684, 1262
Marsch, E., Wiegelmann, T., & Xia, L.-D. 2004, A&A, 428, 629
Marsch, E., Zhou, G.-Q., He, J.-S., & Tu, C.-Y. 2006, A&A, 457, 699
McIntosh, S. W., et al. 2007, ApJ, 654, 650
Orlando, S., Peres, G., & Serio, S. 1995, A&A, 294, 861
Patsourakos, S., & Klimchuk, J. A. 2006, ApJ, 647, 1452
Peter, H. 2001, A&A, 374, 1108
Peter, H. 2007, Adv. Space Res., 39, 1814
Peter, H., & Judge, P. G. 1999, ApJ, 522, 1148
Péter-Suárez, D., Maclean, R. C., Doyle, J. G., & Madjarska, M. S. 2008, A&A, 492, 575
Robb, T. D., & Cally, P. S. 1992, ApJ, 397, 329
Scherrer, P. H., et al. 1995, Sol. Phys., 162, 129
Seehafer, N. 1978, Sol. Phys., 58, 215
Sheeley, N. R., Jr., & Golub, L. 1979, Sol. Phys., 63, 119
Shibata, K., Yokoyama, T., & Shimojo, M. 1996, Adv. Space Res., 17, 197
Stucki, K., et al. 2000, A&A, 363, 1145
Teriaca, L., Banerjee, D., Falchi, A., Doyle, J. G., & Madjarska, M. S. 2004, A&A, 427, 1065
Tian, H., Curdt, W., Marsch, E., & He, J.-S. 2008a, ApJ, 681, L121
Tian, H., Tu, C.-Y., He, J.-S., & Marsch, E. 2007, Adv. Space Res., 39, 1853
Tian, H., et al. 2008b, A&A, 478, 915
Tian, H., et al. 2008c, A&A, 489, 1297
Tsuneta, S., et al. 2008, ApJ, 688, 1374
Tu, C.-Y., Marsch, E., Wilhelm, K., & Curdt, W. 1998, ApJ, 503, 475
Tu, C.-Y., et al. 2005a, Science, 308, 519
Tu, C.-Y., et al. 2005b, ApJ, 624, L133
Uitenbroek, H., Balasubramaniam, K. S., & Tritschler, A. 2006, ApJ, 645, 776
Wang, Y.-M. 2009, Space Sci. Rev., 144, 383
Warren, H. P., & Doschek, G. A. 2005, ApJ, 618, L157
Webb, D. F., Martin, S. F., Moses, D., & Harvey, J. W. 1993, Sol. Phys., 144, 15
Wiegelmann, T., & Neukirch, T. 2002, Sol. Phys., 208, 233
Wiegelmann, T., Xia, L. D., & Marsch, E. 2005, A&A, 432, L1
Wilhelm, K., Dammasch, I. E., Marsch, E., & Hassler, D. M. 2000, A&A, 353, 749
Wilhelm, K., et al. 1995, Sol. Phys., 162, 189
Wuelser, J.-P., et al. 2004, Proc. SPIE, 5171, 111
Xia, L.-D. 2003, PhD thesis, Georg-August-Univ., Göttingen
Xia, L. D., Marsch, E., & Curdt, W. 2003, A&A, 399, L5
Xia, L.-D., Marsch, E., & Wilhelm, K. 2004, A&A, 424, 1025
Yokoyama, T., & Shibata, K. 1996, PASJ, 48, 353